Type I interferon production elicits differential CD4$^+$ T-cell responses in mice infected with *Plasmodium berghei* ANKA and *P. chabaudi*

Running title: Type I interferon and CD4$^+$ T cells in malaria

Mbaya Ntita[†,‡], Shin-Ichi Inoue[†,‡], Jiun-Yu Jian[†,‡], Ganchimeg Bayarsaikhan[†], Kazumi Kimura[†], Daisuke Kimura[†,#], Mana Miyakoda[†,#], Eriko Nozaki[§], Takuya Sakurai[¶], Daniel Fernandez-Ruiz[‖], William R. Heath[‖], Katsuyuki Yui[†,‡,††,‡‡,¶¶]

[†]Division of Immunology, Department of Molecular Microbiology and Immunology, Graduate School of Biomedical Sciences, Nagasaki University, 1-12-4, Sakamoto, Nagasaki 852-8523, Japan.

[‡] Program for Nurturing Global Leaders in Tropical and Emerging Infectious Diseases, Graduate School of Biomedical Sciences, Nagasaki University, 1-12-4, Sakamoto, Nagasaki 852-8523, Japan.

[§]Core Laboratory for Proteomics and Genomics, School of Medicine, Kyorin University, 6-20-2 Shinkawa, Mitaka, Tokyo 181-8611 Japan

[¶]Department of Molecular Predictive Medicine and Sport Science, School of Medicine, Kyorin University, 6-20-2 Shinkawa, Mitaka, Tokyo 181-8611 Japan

[‖] Department of Microbiology and Immunology, The Peter Doherty Institute, The University of Melbourne, Vic, Australia

[††] School of Tropical Medicine and Global Health (TMGH), Nagasaki University, 1-12-4, Sakamoto, Nagasaki 852-8523, Japan.

[‡‡] Institute of Tropical Medicine, Nagasaki University, 1-12-4 Sakamoto, Nagasaki 852-8523, Japan

[¶¶]Corresponding author: Katsuyuki Yui, Division of Immunology, Department of Molecular Microbiology and Immunology, Graduate School of Biomedical Sciences, Nagasaki University, 1-12-4 Sakamoto, Nagasaki 852-8523, Japan; phone: +81-95-819-7070; fax: +81-95-819-7073; e-mail address: katsu@nagasaki-u.ac.jp

[#]Present addresses:Daisuke Kimura: Department of Health, Sports, and Nutrition, Faculty of Health and Welfare, Kobe Women's University, 4-7-2 Minatojima-

nakamachi, Chuo-ku, Kobe, 650-0046, Japan; Mana Miyakoda: Research and Education Center for Drug Fostering and Evolution, School of Pharmaceutical Sciences, Nagasaki University, 1-14 Bunkyomachi, Nagasaki 852-8521, Japan

Number of figures: 6

Keywords: Malaria; cytokine; Th1; Tfh; immunological memory

Abstract

Plasmodium parasites that infect humans are highly polymorphic, and induce various infections ranging from asymptomatic state to life-threatening diseases. However, how the differences between the parasites affect host immune responses during blood-stage infection remains largely unknown. We investigated the $CD4^+$ T-cell immune responses in mice infected with *P. berghei* ANKA (PbA) or *P. chabaudi chabaudi* AS (Pcc) using PbT-II cells, which recognize a common epitope of these parasites. In the acute phase of infection, $CD4^+$ T-cell responses in PbA-infected mice showed a lower involvement of Th1 cells and a lower proportion of $Ly6C^{lo}$ effector $CD4^+$ T cells than those in Pcc-infected mice. Transcriptome analysis of PbT-II cells indicated that type I interferon (IFN)-regulated genes were expressed at higher levels in both Th1- and Tfh-type PbT-II cells from PbA-infected mice than those from Pcc-infected mice. Moreover, IFN-α levels were considerably higher in PbA-infected mice than in Pcc-infected mice. Inhibition of type I IFN signaling increased PbT-II and partially reversed the Th1 over Tfh bias of the PbT-II cells in both PbA- and Pcc-infected mice. In the memory phase, PbT-II cells in PbA-primed mice maintained higher numbers and exhibited better recall response to the antigen. However, recall responses were not significantly different between the infection groups after re-challenge with PbA, suggesting the effect of inflammatory environment by the infection. These observations suggest that the differences in *Plasmodium*-specific $CD4^+$ T-cell responses between PbA- and Pcc-infected mice were associated with the difference in type I IFN production during the early phase of the infection.

Introduction

Malaria is a devastating infectious disease, with an estimated 229 million cases and 409,000 deaths in 2019 (1). The malarial infection is mediated by infectious bites of the *Anopheles* mosquitoes that induce asymptomatic amplification of the parasites in the liver stage, followed by repeated cycles of blood-stage infection. During the blood stage, malarial symptoms that occur vary widely among patients with asymptomatic infection; mild diseases including fever, splenomegaly, and anemia; and severe diseases with life-threatening or lethal developments such as cerebral malaria, acidosis, and severe anemia (2-4). The pathogenesis of infection is determined by the nature of the interaction between parasites and the host immune system. The genomes of *Plasmodium* parasites in the field are highly polymorphic, encoding various pathogenic factors, including *P. falciparum* erythrocyte membrane protein I (PfEMPI) and

Plasmodium interspersed repeat (pir) multigene family proteins. PfEMPI interacts with the adhesion molecules in the host, and pir proteins are expressed in various subcellular localization in the infected RBCs and appear to be associated with virulence of the parasites (5). Host immune responses include innate sensing of pathogen-associated molecular patterns (PAMPs), production of *Plasmodium*-specific antibodies, and the activation of macrophages by specific $CD4^+$ T cells, which are critical for inhibition of the parasite growth during blood-stage infection (2). However, molecular mechanisms that underly the differences in levels and types of malaria symptoms during blood-stage infection are not well-investigated.

Rodent models of malaria infection are valuable tools for investigating the mechanisms underlying the pathology of the disease and the immune responses elicited (2,6-8). As in humans, different species of *Plasmodium* parasites, having different genetic backgrounds, induce distinct diseases in mouse models. *P. chabaudi chabaudi* AS (Pcc) infects both normocytes and reticulocytes, leading to chronic infection by sequestering the infected RBCs in the vascular endothelium, and is used as a model of human infection with *P. falciparum* (6). *Plasmodium berghei* ANKA (PbA) infection induces experimental cerebral malaria (ECM) in susceptible C57BL/6 mice, leading to neurological symptoms and death at relatively low levels of parasitemia (7,8). Differences in disease manifestation can be triggered by differences in parasite factors such as the rate of cell division, ability to infect reticulocytes and normocytes, ability to sequester from the peripheral circulation, and ability to modulate host immune responses. However, host factors restrict the magnitude and quality of the immune responses elicited during infection and are critical in determining disease manifestation.

The T-cell receptor (TCR)-transgenic cell line, PbT-II, expresses αβTCR specific for the *Plasmodium* heat shock protein 90 (hsp90) epitope, which is conserved among PbA, Pcc, *P. yoelii*, and *P. falciparum* in the context of $I\text{-}A^b$ (9,10). Studies on $CD4^+$ T-cell immune responses during infection with Pcc using this model revealed that parasite-specific T cells proliferate extensively and bifurcate to Th1 and Tfh fates within 1 week of infection (11,12). In the chronic phase, these Th1 and Tfh effector PbT-II cells reduce in number but persist mainly in the B-cell zone and maintain the ability to mount a recall IFN-γ response, indicating that they become memory cells (13). Transcriptional and epigenetic studies at a single-cell level have shown that effector Th1 and Tfh cells progressively transit to memory cells over several weeks, during which heterogeneity of the effector cells is partially reset in the memory phase. These studies revealed the dynamic process

of effector and memory $CD4^+$ T-cell development in an infection model of Pcc. However, it is unclear whether $CD4^+$ T cells behave similarly during infection with other species of *Plasmodium* parasites.

In this study, we investigated the antigen-specific $CD4^+$ T-cell immune responses in mice infected with PbA and Pcc using PbT-II cells (9). Since PbT-II cells recognize the hsp90 epitope common to both PbA and Pcc, this study compares the response of $CD4^+$ T cells expressing identical TCRs in two different infection models. We show that $CD4^+$ T-cell responses are less biased toward the Th1 type and that the proportion of $Ly6C^{lo}$ effector $CD4^+$ T cells is lower in mice infected with PbA than in those infected with Pcc. The difference in these $CD4^+$ T-cell responses is associated with the difference in early innate immune responses, including type I interferon (IFN) production.

Methods

Mice and parasites

PbT-II transgenic mice ($CD45.1^+$) have been described previously (9). B6 mice were purchased from SLC (Shizuoka, Japan). PbT-II and B6 mice were maintained in the Laboratory Animal Center of Nagasaki University and were used at the age of 7–14 weeks. All animal experiments were approved by the Institutional Animal Care and Use Committee of Nagasaki University and were conducted in accordance with the guidelines for Animal Experimentation of Nagasaki University.

PbA, originally obtained from R. E. Sinden (Imperial College London, London, UK), was kindly provided by Dr. M. Yuda (Mie University, Japan). Pcc was provided by Dr. R. Culleton (Ehime University, Japan) (6). Parasitized RBCs obtained from the frozen stocks of PbA and Pcc were passed into B6 mice before being used for experimental mouse infection (5×10^4) by intraperitoneal (i.p.) injection. Parasitemia levels were monitored using a light microscope by observing thin blood smears stained with a diff-quick procedure (Sysmex, Kobe, Japan).

An anti-IFN α and β receptor subunit 1 (IFNAR1) blocking monoclonal antibody (mAb; 0.1 mg, MAR1-5A3, Bio X cell, West Lebanon, NH, USA) or rat IgG (0.1 mg) (Sigma Aldrich, St. Louis, MO, USA) was administered via i.p. injection in 100 μL PBS on the day of as well as 2 and 4 days after *Plasmodium* infection as described previously (14), to block type I IFN signaling.

Cell transfer and T-cell priming

$CD4^+$ T cells (>95%) were prepared from the spleen, inguinal, and brachial lymph nodes of PbT-II mice ($CD45.1^+$) using anti-CD4 IMag (BD Biosciences, San Diego, CA, USA) according to the manufacturer's instructions. PbT-II cells (1×10^6/250 µL) in PBS were transferred intravenously into B6 ($CD45.2^+$) mice through the lateral tail vein one day before infection. To prime mice with *Plasmodium* infection, mice were infected with PbA or Pcc, and chloroquine was administered (10 µg/g mouse weight; Sigma-Aldrich) via i.p. injection for 7 days and sulfadiazine (30 mg/L; Sigma-Aldrich) was administered through drinking water for 10 days between 6 and 15 days post-infection, as previously described (15). Bone marrow derived dendritic cells (BM-DCs) were prepared as described previously with some modifications (16). Briefly, BM cells were cultured for 8 days in the presence of GM-CSF (200U/mL) (Biolegend, San Diego, CA, USA) and LPS (500ng/ml) (*Escherichia coli* 0127:B8, Sigma-Aldrich) for the last 24 h. After washing, BM-DCs were pulsed with PbT-II peptide (DNQKDIYYITGESINAVS) (2 µg/mL) (Sigma-Aldrich) (10) at 37°C for 2 hrs, washed, resuspended in 3×10^5 cells/250µL PBS, and transferred intravenously (i.v.) into each mouse.

Flow cytometry

RBCs from the harvested spleens were lysed using Gey's solution, and a single-cell suspension was prepared. The cells were stained with mAbs or their isotype controls at 4 °C for 30 min. The following antibodies were used: BV510-anti-CD3 (145-2C11), BV711-anti-CD4 (GK1.5), APCcy7-anti-CD45.1 (A20), BV605-anti-CD45.2 (104), FITC-anti-CD11a (M17/4), BV421-anti-CD49d (9C10), PEcy7-anti-CXCR5 (L138D7), APC-anti-Ly6C (HK1.4), PE-anti-PD-1 (J43.1) (TONBO), PEcy7-anti-PD-1 (29F.1A12), PE-anti-CD62L (MEL-14), FITC-anti-CD44 (IM7), PE-anti-CD127 (A7R34), APC-anti-KLRG1 (2F1/KRG1) mAbs. All the mAbs were purchased from Biolegend unless otherwise specified. To exclude dead cells, 7-aminoactinomycin D (7AAD) was added before analysis. For intracellular staining of transcription factors, cells were stained with BV510-anti-CD3, BV711-anti-CD4, APCcy7-anti-CD45.1, APC-anti-CXCR5, or APC-anti-Ly6C mAb, fixed, and permeabilized using Cytofix/Cytoperm buffer (eBioscience) as described previously (17). After incubation with anti-CD16/CD32 mAb (2.4G2) for 15 min to block Fc receptors, the cells were stained with PECy7-anti-Tbet (4B10), PE-anti-Bcl6 (7D1), or PE-anti-Tcf-1 (S33-966) (BD Biosciences, Franklin Lakes, NJ, USA)

mAb and analyzed using a BD LSRFortessa X-20 instrument (BD Biosciences) and the FlowJo software (Tree Star, Ashland, OR, USA).

Cell culture and intracellular cytokine staining

Spleen cells were harvested, RBCs were lysed using Gey's solution, and cells were suspended in RPMI-1640 medium supplemented with 10% FCS, 2 mM glutamine, penicillin/streptomycin, 2-mercaptoethanol (5×10^{-5} M), non-essential amino acids (0.1 mM), and sodium pyruvate (1 mM). Splenocytes (3×10^6/well) were cultured in 24-well plates with PbT-II peptide (1 μg/mL) or phorbol 12-myristate 13-acetate (PMA; 50 ng/mL) and ionomycin (0.5 μg/mL) for 4 h in the presence of Golgi stop (BD Biosciences). After incubation with anti-CD16/CD32 mAb for 15 min, cells were stained with BV510-anti-CD3, BV711-anti-CD4, APCcy7-anti-CD45.1 mAbs, fixed, and permeabilized using Cytofix/Cytoperm buffer (BD Biosciences). Cells were intracellularly stained with AF488-anti-IFN-γ (XMG1.2), PE-anti-tumor necrosis factor-α (TNF-α) (MP6-XT22), or APC-anti-IL-2 (JES6-5H4) mAbs and analyzed using BD LSRFortessa X-20 instrument (BD Biosciences) and the FlowJo software (Tree Star).

ELISA

The spleen lysate was prepared as previously described, with slight modifications (18). In brief, spleens were harvested in cold PBS (1 mL), weighed, and suspended in ice-cold PBS containing Igepal CA-630 nonionic detergent (0.1%, Sigma-Aldrich) and protease inhibitor cocktail (50 μL/10 mg tissue) (P8340, Sigma-Aldrich) for 10 min. Spleens were crushed and resuspended; the lysate was incubated at 4 °C for 30 min and centrifuged at 14,000 × *g* for 5 min; the obtained supernatant was stored at -80 °C until use. The level of IFN-α was determined using an ELISA kit (VeriKine Mouse IFN-α, PBL Assay Science, Piscataway, NJ, USA). IFN-γ levels were determined using sandwich ELISA with a set of anti-IFN-γ (R4-6A2) and biotin-anti-IFN-γ (XMG1.2) mAbs, as previously described (19).

Levels of *Plasmodium*-specific IgM, IgG1, IgG2b, and IgG2c were determined by ELISA, as previously described (15). ELISA plates (Nunc MaxiSorp ®, Thermo Fisher Scientific) were coated with the freeze-thaw lysate of PbA or Pcc (1×10^6 iRBC equivalent/well) in PBS at room temperature for 2 h. After washing three times with PBS containing Tween

20 (0.02%), the coated plates were blocked with PBS containing FCS (10%) and Tween-20 (0.02%) for 30 min at room temperature. After washing, serial dilutions of sera (1/20–1/1280) were added, and the plates were incubated overnight at 4 °C. After washing, plates were incubated with biotin-conjugated rabbit anti-mouse IgM, IgG1, IgG2b (ZyMED, San Francisco, CA, USA), or IgG2c (Bethyl Laboratories, Montgomery, TX, USA) antibodies for 1 h, washed, and incubated with alkaline phosphatase-conjugated streptavidin (Jackson ImmunoResearch, West Grove, PA, USA) for 30 min. After washing, 4-nitrophenyl phosphate disodium salt hexahydrate (Sigma-Aldrich, 1 mg/mL) was added to each well, and the absorbance was read at 405 nm using an iMark Microplate Absorbance Reader (Bio-Rad, Hercules, CA, USA).

Cell sorting and microarray analysis

Spleens were harvested, RBCs were lysed using Gey's solution, and cells were stained with APC-anti-CD45.1 for 30 min at 4 °C. After washing, the cells were incubated with anti-APC magnetic-activated cell sorting (MACS) microbeads (Miltenyi Biotec, Gladbach, Germany) and PbT-II cells enriched using Auto-MACS (Miltenyi Biotec). These cells were stained with PEcy7-anti-CD3Ɛ, APCcy7-anti-CD4, FITC-anti-CD11a, PE-anti-CD49d mAbs and 7AAD, and $CD11a^{hi}CD49d^{hi}$ and $CD11a^{hi}CD49d^{lo}$ PbT-II cells were sorted using a BD FACSAria instrument (BD Biosciences). Total RNA was extracted from the sorted cells using a RNeasy Mini kit (Qiagen, Hilden, Germany) and subjected to microarray analysis, as described previously (12). Briefly, complementary DNA (cDNA) generated from the RNA was amplified, fragmented, and labeled using a GeneChip 3' IVT Pico Kit (Applied Biosystems, Foster City, CA, USA). Gene-expression profiles of the amplified cDNA (6.6 μg/array) were determined using the Clariom S Array (Applied Biosystems). Gene expression levels were analyzed using the Transcriptome Analysis Console software (Invitrogen, Carlsbad, CA, USA). Differentially expressed genes (DEGs) were listed for those with at least 2-fold changes and p values <0.05, comparing PbT-II cells from PbA- and Pcc-infected mice. Principal component analysis (PCA) was performed, and graphs were extracted from Transcription Analysis Console software (Invitrogen). GraphPad Prism software (GraphPad, San Diego, CA, USA) was used to generate a volcano plot. The heatmap of the gene lists were generated using online software Heatmapper (20). For gene set enrichment analysis (GSEA), software from the Broad Institute (Massachusetts Institute of Technology, Cambridge, MA, USA) was used, and the gene sets were compared with those from the Molecular Signatures Database (MSigDB) to find out significantly enriched gene sets (21). The microarray datasets

generated for Pcc infection is available at GSE/microarray data (GSE153600) (12) and for PbA infection during this study at (GSE179860).

Statistical analysis

Data are shown as the mean ± standard deviation (SD). Statistical analyses were performed using GraphPad Prism software version 8 (GraphPad, San Diego, CA, USA). Comparison of two groups was performed using a two-tailed unpaired *t*-test. Pearson's correlation test was used to analyze the correlation between parasitemia levels and phenotype. Two-way analysis of variance (ANOVA) with Bonferroni's correction test or multiple *t*-tests was used to analyze cytokine production and specific antibody responses, respectively. Both tests were used at a significance level of 0.05 ($p < 0.05$).

Results

$CD4^+$ T cells in PbA-infected mice show less Th1 bias than those in Pcc-infected mice

First, we compared the activation and differentiation of $CD4^+$ T cells during infection with PbA and Pcc using $CD4^+$ T cells from PbT-II transgenic mice that express TCR specific for the hsp90 epitope common to these parasites (9). B6 mice were injected with PbT-II cells, uninfected or infected with PbA or Pcc, and the phenotype of splenic T cells was examined 7 days after the infection (Fig. 1, Fig. S1). This date was chosen, since we begin to find death of PbA-infected B6 mice due to ECM (15). We observed that the proportion of PbT-II cells in $CD4^+$ T cells was significantly higher in PbA-infected mice than in Pcc-infected mice (Fig. 1A). However, the total number of PbT-II cells in the spleen was lower in the PbA-infected mice because of an increase in the number of splenocytes in Pcc-infected mice. CD11a and CD49d are upregulated in activated $CD4^+$ T cells and $CD11a^{hi}CD49d^{hi}$ marks Th1-type $CD4^+$ T cells in *Plasmodium* infected mice (12). The proportion of $CD11a^{hi}CD49d^{hi}$ cells in PbT-II cells was significantly lower in PbA-infected mice than in Pcc-infected mice (Fig. 1A). Ly6C is a marker that distinguish memory cells from effector Th1 cells and $LyC6^{lo}$ cells have high memory potential (22, 23). The proportion of $Ly6C^{lo}$ cells was lower in PbA-infected mice, suggesting the lower level of memory PbT-II cells in these mice (Fig. 1A, Fig. S1B). The proportion of $PD\text{-}1^+CXCR5^+$ Tfh cells was not significantly different between the two groups. PbT-II cells are divided into two populations based on the expression of T-bet and Tcf-1: $T\text{-}bet^{hi}Tcf\text{-}1^{lo}$ cells represent Th1 types and $T\text{-}bet^{lo}Tcf\text{-}1^{hi}$ are Tfh-like cells (12). The proportion of

T-bet^{hi}Tcf-1^{lo} cells in PbA-infected mice was lower than that in Pcc-infected mice, confirming the reduced Th1 bias in PbA-infected mice in both PbT-II and host CD4^{+} T cells (Fig. 1B, Fig. S1C). The proportion of Bcl-6^{hi} cells was not significantly different between the two groups. We further examined the proportion of T-bet^{hi}Tcf-1^{lo} PbT-II cells that were Ly6C^{lo} since the Ly6C^{lo}T-bet^{hi} population was suggested as a precursor of memory CD4^{+} T cells (22). The proportion of Ly6C^{lo} cells in PbA-infected mice was lower than that in Pcc-infected mice in both T-bet^{hi}Tcf-1^{lo} and T-bet^{lo}Tcf-1^{hi} PbT-II and the host CD4^{+} T cells (Fig. 1B, Fig. S1C). In PbA-infected mice and in malaria-exposed children, CXCR3^{+}T-bet^{+} Th1-like Tfh are increased (24, 25). Bcl-6^{+} Tfh-like cells in PbA or Pcc-infected mice express T-bet (Fig. S1C), hence we examined CXCR3 expression of PbT-II and host CD4^{+} T cells cells (Fig. S2). The expression of CXCR3 was upregulated in Tfh in both PbA and Pcc infection, with PbA-infected mice exhibiting higher expressions. We thus confirmed that Tfh induced by PbA and Pcc infection exhibit Th1-like phenotype.

Next, we evaluated the correlation between the phenotype of CD4^{+} T cells and the levels of parasitemia (Fig. 1C, Fig. S1D) to evaluate the contribution of parasitemia levels to the differentiation of CD4^{+} T cells. Seven days after infection, levels of parasitemia in PbA-infected mice were 8.6% ± 1.9%, while parasitemia levels varied among the Pcc-infected mice in the range of 23.6% ± 15.9%. However, in both cases of infections, there was no significant correlation between the levels of parasitemia and the proportions of CD11a^{hi}CD49d^{hi} or T-bet^{hi}Tcf1^{lo} cells in both PbT-II cells and host CD4^{+} T cells (Fig. 1C, Fig S1D). In addition, the proportion of Ly6C^{lo} cells within T-bet^{hi}Tcf1^{lo} or T-bet^{lo}Tcf1^{hi} cells was barely affected by parasitemia levels in PbT-II cells and host CD4^{+} T cells.

We then evaluated the function of PbT-II cells by assessing the patterns of intracellular cytokine staining (Fig. 2). The proportions of PbT-II cells producing either IFN-γ or both IFN-γ and TNF-α in response to the antigenic peptide were lower in PbA-infected mice than in Pcc-infected mice, consistent with the phenotype of these cells, indicating that CD4^{+} T cells are less Th1-biased in PbA-infected mice than in Pcc-infected mice. The levels of IL-10-producing PbT-II cells were less than 5% in both PbA- and Pcc-primed mice (data not shown). Our observations collectively suggest that during acute infection

with PbA, antigen-specific $CD4^+$ T cells exhibited lower expansion, less Th1-biased responses, and lower levels of $Ly6C^{lo}$ cells when compared with Pcc-infected mice.

Transcriptome analysis of PbT-II cells revealed a higher type I IFN response in PbA-infected mice than in Pcc-infected mice

Next, we compared the transcriptomes of $CD11a^{hi}CD49d^{hi}$ and $CD11a^{hi}CD49d^{lo}$ PbT-II cells in mice infected with PbA and Pcc (Fig. 3, Fig. S3). B6 mice were transferred with PbT-II cells and were infected with PbA. $CD11a^{hi}CD49d^{hi}$ and $CD11a^{hi}CD49d^{lo}$ PbT-II cells were sorted 7 days after the infection. Microarray analysis of RNA prepared from these cells was compared with data obtained previously from $CD11a^{hi}CD49d^{hi}$ and $CD11a^{hi}CD49d^{lo}$ PbT-II cells from Pcc-infected mice and $CD11a^{lo}CD49d^{lo}$ PbT-II cells from uninfected mice containing PbT-II cells (12). PCA separated all five populations; principal components 1 and 2 separated $CD11a^{lo}CD49d^{lo}$, $CD11a^{hi}CD49d^{hi}$, $CD11a^{hi}CD49d^{lo}$ populations; and principal component 3 distinguished cells from PbA- and Pcc-infected mice (Fig. 3A). The number of DEGs (log2 fold change > 2, $p < 0.05$) between PbA- and Pcc-infected mice was 1,350 and 1,132 in $CD11a^{hi}CD49d^{hi}$ and $CD11a^{hi}CD49d^{lo}$ cells, respectively, with 287 DEGs common to both populations (Fig. 3B). Among the top 10 DEGs of $CD11a^{hi}CD49d^{hi}$ PbT-II in PbA-infected mice, *Usp18, Oas2, Oas1g, Irf7, Dhx58, Oas1a,* and *Parp12* were related to the type I IFN signaling pathway (Fig. 3C, D). Most of these genes were also expressed at higher levels in the $CD11a^{hi}CD49d^{lo}$ PbT-II subsets in PbA-infected mice. As expected, Th1 differentiation-related genes were upregulated, while Tfh-related genes were downregulated in $CD11a^{hi}CD49d^{hi}$ PbT-II cells compared with $CD11a^{hi}CD49d^{lo}$ PbT-II cells in both PbA- and Pcc-infected mice. Gene ontology (GO) analysis of the DEGs between PbA- and Pcc-infected mice showed enrichment of GO terms describing response to IFN-α, type I IFN signaling pathway, and response to type I IFN being upregulated in both $CD11a^{hi}CD49d^{hi}$ and $CD11a^{hi}CD49d^{lo}$ PbT-II cells (Fig. 3E). GSEA showed that gene sets related to innate immunity and type I IFN-related genes were significantly enriched in $CD11a^{hi}CD49d^{hi}$ PbT-II cells from PbA-infected mice compared with those from Pcc-infected mice (Fig. 3F). Similar results were obtained in the GSEA of $CD11a^{hi}CD49d^{lo}$ PbT-II cells. Since type I IFN-regulated genes were the major DEGs in PbT-II cells from PbA- and Pcc-infected mice, we examined the expression of IFN-α in the spleen after infection with PbA or Pcc (Fig. 3G). The level of IFN-α in the spleen was undetectable 1.5 and 3 days after infection with either PbA or Pcc (data not shown) and became detectable 5 days after infection. Its level was much

higher in PbA-infected mice than in Pcc-infected mice, whereas IFN-γ levels were not significantly different, suggesting a link between IFN-α production in the innate immune response and subsequent $CD4^+$ T-cell responses. Collectively, we observed that PbA infection induced type I IFN response at higher levels when compared with Pcc-infected mice and influenced the expression of related genes in activated $CD4^+$ T cells.

Inhibition of type I IFN signaling modulates the response of $CD4^+$ T cells

We hypothesized that the difference in type I IFN production between PbA- and Pcc-infected mice regulates the development of $CD4^+$ T cells. We examined the effect of inhibition of type I IFN signaling by anti-IFNAR1 antibody treatment on $CD4^+$ T-cell response 7 days after *Plasmodium* infection to test this possibility (Fig. 4, Fig. S4). In PbA-infected mice, type I IFN inhibition increased the total number of PbT-II without significant effect on parasitemia levels (Fig. 4A, B). The proportion of $CD11a^{hi}CD49d^{hi}$, $Ly6C^{lo}$ and $T\text{-}bet^{hi}Tcf\text{-}1^{lo}$ PbT-II cells increased while that of $T\text{-}bet^{lo}Tcf\text{-}1^{hi}$ PbT-II cells decreased by the treatment, suggesting the shift to Th1 development in the absence of type I IFN signaling (Fig. 4C, D). In the host $CD4^+$ T cells, the proportion of $T\text{-}bet^{lo}Tcf\text{-}1^{hi}$ cells was reduced (Fig. 4D). Moreover, the levels of $Ly6C^{lo}$ cells were increased in both $T\text{-}bet^{hi}Tcf\text{-}1^{lo}$ and $T\text{-}bet^{lo}Tcf\text{-}1^{hi}$ PbT-II and host $CD4^+$ T cells (Fig. 4C, D). The treatment with anti-IFNAR1 antibody, however, did not affect ECM development, as both treated and untreated mice succumbed to death by day 8 (data not shown), unlike a previous study reporting that anti-IFNAR1 treatment caused a reduction in parasitemia and provided protection against fatal disease (26). This discrepancy could be due to the difference in the method of the challenge infection. We infected mice i.p. with 5×10^4 iRBCs, while Haque et al infected mice i.v. with 10^5 iRBCs (26). Alternatively, the difference could derive from the PbA parasites that have been maintained in the two laboratories. We also examined the effect of type I IFN inhibition in Pcc-infected mice with similar but milder effects (Fig. S4). The total number of PbT-II cells showed a tendency to increase, although the difference was not statistically significant (Fig. S4B). The proportion of $T\text{-}bet^{lo}Tcf\text{-}1^{hi}$ cells was reduced and that of $Ly6C^{lo}$ cells was increased in both $T\text{-}bet^{hi}Tcf\text{-}1^{lo}$ and $T\text{-}bet^{lo}Tcf\text{-}1^{hi}$ PbT-II and host $CD4^+$ T cells, although the extent was lower than in PbA-infected mice (Fig. S4D). Taken together, we confirmed that inhibition of type I IFN increased PbT-II cell number, increased Th1 cells, reduced the proportion of Tfh-like cells, and increased $Ly6C^{lo}$ $CD4^+$ T cells in PbA-infected mice. The same treatment had similar but milder effects in Pcc-infected mice. These results are

consistent with the expression of higher levels of type I IFN-related genes and IFN-α production in PbA-infected mice when compared with Pcc-infected mice.

Memory CD4$^+$ T cells generated by PbA or Pcc infection

We next analyzed the memory CD4$^+$ T cells induced by PbA and Pcc infections. B6 mice were transferred with PbT-II cells, infected with PbA or Pcc, and treated with an anti-*Plasmodium* drug to exclude the effect of active infection on the immune responses. Three weeks after infection, the amount of CD4$^+$ T cells were examined in mice. The proportion of CD4$^+$ T cells and the total number of PbT-II cells were higher in PbA-infected mice than in Pcc-infected mice, suggesting better maintenance of PbT-II cells in PbA-infected mice (Fig. 5A). There were no significant differences in the proportions of CD11a^{hi}CD49d^{hi}, Ly6C^{hi}, Tfh (CXCR5$^+$PD-1$^+$), CD127$^+$KLRG1$^-$, T-bet^{hi}Tcf-1^{lo}, and Bcl6$^+$CXCR5$^+$ PbT-II cells (Fig. 5A, C). However, the proportion of central memory (CD44$^+$CD62L$^+$) PbT-II cells were lower, while effector memory (CD44$^+$CD62L$^-$) PbT-II cells were higher in PbA-primed mice when compared with Pcc-primed mice (Fig. 5B). We also examined the levels of *Plasmodium*-specific antibodies using crude lysates of PbA-infected and Pcc-infected RBCs (Fig. 5C). Serum levels of anti-PbA IgG1 and IgG2b in PbA-infected mice were higher than those in Pcc-infected mice. Similarly, serum levels of anti-Pcc IgG2c and IgG2b in Pcc-infected mice were higher than those in PbA-infected mice. These observations collectively led us to conclude that there was no significant difference in the levels of anti-*Plasmodium* antibodies between PbA-infected and Pcc-infected mice, which was consistent with the similar levels of Tfh in both groups.

To examine the recall response of the memory CD4$^+$ T cells, mice were transferred with PbT-II cells, infected with PbA or Pcc, treated with anti-*Plasmodium* drug, and were immunized with BM-DCs pulsed with PbT-II peptide (Fig. 6A). The proportion of PbT-II cells in peripheral blood of PbA-primed mice was higher than those of Pcc-primed mice early after infection and was reduced to the levels similar to Pcc-infected mice after 8 days of immunization (Fig. 6B). We did not find any significant difference in PbT-II cell number in the spleen 14 days after immunization, although the number in PbA-primed mice showed higher tendency (Fig. 6C). We next challenged the primed mice with PbA 21 days after the primary infection (Fig. 6D-F) (15). Although the levels of parasitemia after infection with PbA was slightly higher in PbA-primed mice than in Pcc-primed mice, the proportion and the total number of PbT-II cells in the spleen of PbA-challenged mice were not significantly different (Fig. 6D, E). Additionally, there

was no significant difference in the proportion of CD11a^{hi}CD49d^{hi}, Tfh, T-bet^{hi}Tcf-1^{lo}, and Bcl6^{+}CXCR5^{+} PbT-II cells between the PbA- and Pcc-primed mice after challenge infection with PbA. Collectively, the levels of memory PbT-II cells were higher in PbA-primed mice than in Pcc-primed mice, and PbT-II cells in PbA-primed mice induced higher response to peptide immunization than those in Pcc-primed mice. However, there was no statistical differences in terms of PbT-II cell number and phenotype after the challenge infection with PbA.

Discussion

In this study, we show quantitative and qualitative differences in *Plasmodium*-specific CD4^{+} T-cell immune responses between the acute phases of PbA and Pcc infections. To our knowledge, this is the first study to directly compare the T-cell immune responses to infection with different strains of *Plasmodium* and revealed the critical roles of type I IFNs in shaping subsequent host immune responses. The *IFNAR1* gene polymorphism is associated with an increased risk of cerebral malaria in *P. falciparum*-infected patients in Gambia and Angola (27, 28). Neutrophils activated by type I IFN are recruited and damage liver in patients infected with *P. vivax* (29). In the mouse model of PbA infection, IFN-α/β is inhibitory to the adaptive immune responses, as shown using mice deficient in the IFNAR1 receptor or mice in which its function is inhibited with an anti-IFNAR1 antibody that exhibits better parasite control and lacks neurological symptoms or ECM development (14, 26, 27). In this study, we showed that IFN-α was produced at higher levels in the spleen of PbA-infected mice than in Pcc-infected mice, suggesting that the differences in CD4^{+} T-cell responses during infection with PbA and Pcc are at least partly due to the difference in type I IFN production. However, anti-IFNAR1 antibody treatment did not improve parasitemia nor fatal ECM. In addition, the level of IFN-α that we detected in spleen of PbA-infected mice was nearly 10 times below the level of a previous study (14). We think that these discrepancies are likely due to the differences in the methods and parasites used. The reduced type I IFN response may be related to the lower effects of anti-IFNAR1 blockade on the protective immune response in our PbA-infection study. Despite these discrepancies, our results on CD4^{+} T cell phenotype and function corroborate the findings from previous studies and suggest that the difference in pathogenicity of PbA and Pcc infections partially relies on the difference in the magnitude of type I IFN response induced by these species of *Plasmodium* parasites.

Plasmodium-induced type I IFN signaling modulates $CD4^+$ T-cell immune responses via direct and indirect pathways. In the direct pathway, $CD4^+$ T-cell intrinsic IFNAR1 signaling induces T-bet/Blimp-1 in specific $CD4^+$ T cells and promote development of type I regulatory T cells that produce IFN-γ and IL-10, which restricts accumulation of Tfh during *P. yoelii* 17XNL infection (30). $CD8^+$ intrinsic IFNAR1 signaling is also crucial for the pathogenicity inducing ECM in PbA infection (27). In the indirect pathway, type I IFN induces activation of conventional DCs and upregulates PD-L2 and IL-10 production, inhibiting Th1 and Tfh differentiation and proliferation of $CD4^+$ T cells in *P. yoelii* 17XNL and Pcc models (14, 31). Inhibition of the type I IFN pathway enhances $CD4^+$ T-cell activation and improves protective humoral immune response. Our study revealed that the most highly upregulated genes in both $CD49d^{hi}$ Th1-type and $CD49d^{lo}$ Tfh-like PbT-II cells in PbA-infected mice were type I IFN-related genes when compared with Pcc-infected mice, suggesting how IFNAR1 signaling intrinsically affects both types of $CD4^+$ cells. Therefore, type I IFNs produced after *Plasmodium* infection not only shift the Th1/Tfh balance of $CD4^+$ T cells, but also the gene expression within each of these T cells, potentially affecting their function in the protection and pathogenesis of malaria. Thus, the effects of type I IFN on the immune cells during infection are recorded in the transcriptional signature of individual $CD4^+$ T cells and affect subsequent immune status, protection, and pathogenesis of the disease.

Plasmacytoid DCs are the major source of IFN-α/β in *Plasmodium* infections (14, 32-34). However, mechanisms leading to the production of type I IFN might be different among *Plasmodium* strains. Haque et al. showed that IFN-α/β production is maximum at 4 days after infection with PbA and inhibits the function of conventional DCs to prime IFN-γ-producing $CD4^+$ T cells (14). Subsequently, conventional DCs also produce type I IFNs in an IFN-α/β-dependent manner, forming a feedforward loop of type I IFN signaling (14). Other groups reported that the levels of serum IFN-α/β peaked 1-1.5 d after infection with *P. yoelii* YM, and that pDCs recognize the parasite in TLR7-mediated pathway and produce IFN-α/β (33, 34). The activation of this pathway requires priming of pDCs by macrophages upon STING-mediated sensing of parasites. In human cells, it is reported that AT-rich *Plasmodium* DNA stimulate type I IFN production via GMP-AMP synthase (cGAS)-STING-dependent pathway (35). We compared $CD4^+$ T-cell immune responses in infection models of PbA and Pcc in parallel under the same conditions and found that IFN-α/β is produced in PbA-infected mice at higher levels than in Pcc-infected mice. AT contents of PbA and Pcc genomes are similar, with 76.4% and 78.0%, respectively,

(www.ncbi.nlm.nih.gov) and thus cannot explain the difference in IFN-α/β production in both infections. It will be interesting to investigate the nature of PAMPs that stimulate differential type I IFN production during *Plasmodium* infection.

Ly6C is a marker of $CD4^+$ T cells that distinguishes between those with high memory potential and terminal effectors. $Ly6C^{lo}$ Th1 effector cells have a transcriptional signature similar to memory $CD4^+$ T cells and display greater longevity and proliferative response to secondary infection, while $Ly6C^{hi}$ effector $CD4^+$ T cells are more terminally differentiated Th1 cells (22, 36). In addition, type I IFN has been reported to promote the expression of Ly6C on $CD4^+$ T cells (23, 37). In this study, we showed that the proportion of $Ly6C^{lo}$ PbT-II cells was increased by the inhibition of type I IFN in both PbA- and Pcc-infected mice. Consistently, the number of $Ly6C^{lo}$PbT-II cells in the spleen with acute PbA infection was lower than that with Pcc infection. In the memory phase, however, memory PbT-II cells in PbA-primed mice was higher in number, contained more central memory phenotype, and exhibited higher recall response in response to antigen-loaded BM-DCs when compared with those in Pcc-primed mice. In contrast to the peptide immunization, PbT-II cell numbers and phenotypes of PbA- and Pcc-primed mice were not significantly different after re-challenge with PbA. This observation is consistent with the single-cell analysis of PbT-II cells, which revealed that the epigenomic and transcriptomic heterogeneity of $CD4^+$ T cells during the effector phase was partially reset and the differences gradually and partially diminished during the chronic phase (13). The activation of innate immunity, cell–cell interaction and cytokine environment including type I IFN might modify the magnitude of memory $CD4^+$ T cells after *Plasmodium* infection (38). These features suggest the complexity of the generation and maintenance of $CD4^+$ T-cell memory in malaria. In our study, $Ly6C^{lo}$ phenotype was unable to predict the magnitude of memory $CD4^+$ T cells in the comparison between PbA- and Pcc-infected mice.

Plasmodium-specific $CD4^+$ T cells bifurcate to Th1 and Tfh-like cells after activation (11, 12). *Plasmodium*-specific $CD4^+$ T cells in PbA-infected mice are less biased toward Th1 than those in Pcc-infected mice. This bias partially depends on type I IFNs since inhibition of IFNAR1 signaling partially moves the Th1/Tfh bias toward the direction of Th1 dominance. Monocytes and macrophages that are recruited to the spleen may also support fate decisions in activated $CD4^+$ T cells during *Plasmodium* infection, as

suggested previously (11). *Plasmodium* parasites are genetically diverse and are capable of inducing distinct inflammatory environment and adaptive immunity leading to infections ranging from asymptomatic to life-threatening diseases. In this study, we showed that the magnitude and quality of $CD4^+$ T-cell immune responses are affected by differences in the infecting parasites. In particular, type I IFN produced during the acute phase of infection has critical roles in shaping $CD4^+$ T-cell functionality. Further studies may determine the critical factors that dictate the difference in the fate decision during activation and differentiation of specific $CD4^+$ T cells during PbA and Pcc infections. These studies will shed light on developing next-generation malaria vaccines and therapeutics to improve protective immune responses to control severe malaria.

Acknowledgments

We thank Dr. R. Culleton for providing Pcc and Dr. M. Yuda for providing PbA. We also thank N. Kawamoto for providing technical assistance. We thank Editage for English language editing. MN thanks the Otsuka Toshimi Scholarship Foundation for their financial support during his PhD study.

Funding sources

This work was supported by grants-in-aid for scientific research from the Japan Society for the Promotion of Science (18K19456, 19H03460) to KY.

References

1 WHO. 2020. World malaria reprot 2020. *https://www.who.int/publications/i/item/world-malaria-report-2019*.

2 Schofield, L. and Grau, G. E. 2005. Immunological processes in malaria pathogenesis. *Nat Rev Immunol* 5:722.

3 Crompton, P. D., Moebius, J., Portugal, S., Waisberg, M., Hart, G., Garver, L. S., Miller, L. H., Barillas-Mury, C., and Pierce, S. K. 2014. Malaria immunity in man and mosquito: insights into unsolved mysteries of a deadly infectious disease. *Annu Rev Immunol* 32:157.

4 Su, X. Z., Lane, K. D., Xia, L., Sa, J. M., and Wellems, T. E. 2019. *Plasmodium* genomics and genetics: new insights into malaria pathogenesis, Drug Resistance, Epidemiology, and Evolution. *Clin Microbiol Rev* 32.

5 Yui, K. and Inoue, S. I. 2021. Host-pathogen interaction in the tissue environment during *Plasmodium* blood-stage infection. *Parasite Immunol* 43:e12763.

6 Stephens, R., Culleton, R. L., and Lamb, T. J. 2012. The contribution of *Plasmodium chabaudi* to our understanding of malaria. *Trends Parasitol* 28:73.

7 Howland, S. W., Claser, C., Poh, C. M., Gun, S. Y., and Renia, L. 2015. Pathogenic $CD8^+$ T cells in experimental cerebral malaria. *Semin Immunopathol* 37:221.

8 Ghazanfari, N., Mueller, S. N., and Heath, W. R. 2018. Cerebral malaria in mouse and man. *Front Immunol* 9:2016.

9 Fernandez-Ruiz, D., Lau, L. S., Ghazanfari, N., Jones, C. M., Ng, W. Y., Davey, G. M., Berthold, D., Holz, L., Kato, Y., Enders, M. H., Bayarsaikhan, G., Hendriks, S. H., Lansink, L. I. M., Engel, J. A., Soon, M. S. F., James, K. R., Cozijnsen, A., Mollard, V., Uboldi, A. D., Tonkin, C. J., de Koning-Ward, T. F., Gilson, P. R., Kaisho, T., Haque, A., Crabb, B. S., Carbone, F. R., McFadden, G. I., and Heath, W. R. 2017. Development of a novel $CD4^+$ TCR transgenic line that reveals a dominant role for $CD8^+$ dendritic cells and CD40 signaling in the generation of helper and CTL responses to blood-stage malaria. *J Immunol* 199:4165.

10 Enders, M. H., Bayarsaikhan, G., Ghilas, S., Chua, Y. C., May, R., N de Menezes, M., Ge, Z., Tan, P. S., Cozijnsen, A., Mollard, V., Yui, K., McFadden, G. I., Lahoud, M. H., Caminschi, I., Purcell, A. W., Schittenhelm, R. B., Beattie, L., Heath, W. R., and Fernandez-Ruiz, D. 2021. Plasmodium berghei Hsp90 contains a natural immunogenic I-A^b-restricted antigen common to rodent and human *Plasmodium* species. *Currt Res Immunol*. In Press.

11 Lonnberg, T., Svensson, V., James, K. R., Fernandez-Ruiz, D., Sebina, I., Montandon, R., Soon, M. S., Fogg, L. G., Nair, A. S., Liligeto, U., Stubbington, M. J., Ly, L. H., Bagger, F. O., Zwiessele, M., Lawrence, N. D., Souza-Fonseca-Guimaraes, F., Bunn, P. T., Engwerda, C. R., Heath, W. R., Billker, O., Stegle, O., Haque, A., and Teichmann, S. A. 2017. Single-cell RNA-seq and computational analysis using temporal mixture modelling resolves Th1/Tfh fate bifurcation in malaria. *Sci Immunol* 2.

12 Jian, J. Y., Inoue, S. I., Bayarsaikhan, G., Miyakoda, M., Kimura, D., Kimura, K., Nozaki, E., Sakurai, T., Fernandez-Ruiz, D., Heath, W. R., and Yui, K. 2021. CD49d marks Th1 and Tfh-like antigen-specific $CD4^+$ T cells during *Plasmodium chabaudi* infection. *Int Immunol*. In press.

13 Soon, M. S. F., Lee, H. J., Engel, J. A., Straube, J., Thomas, B. S., Pernold, C. P. S., Clarke, L. S., Laohamonthonkul, P., Haldar, R. N., Williams, C. G., Lansink, L. I. M., Moreira, M. L., Bramhall, M., Koufariotis, L. T., Wood, S., Chen, X., James, K. R., Lonnberg, T., Lane, S. W., Belz, G. T., Engwerda, C. R., Khoury, D. S., Davenport, M. P., Svensson, V., Teichmann, S. A., and Haque, A. 2020. Transcriptome dynamics of $CD4^+$ T cells during malaria maps gradual transit from effector to memory. *Nat Immunol* 21:1597.

14 Haque, A., Best, S. E., Montes de Oca, M., James, K. R., Ammerdorffer, A., Edwards, C. L., de Labastida Rivera, F., Amante, F. H., Bunn, P. T., Sheel, M., Sebina, I., Koyama, M., Varelias, A., Hertzog, P. J., Kalinke, U., Gun, S. Y., Renia, L., Ruedl, C., MacDonald, K. P., Hill, G. R., and Engwerda, C. R. 2014. Type I IFN signaling in $CD8^-$ DCs impairs Th1-dependent malaria immunity. *J Clin Invest* 124:2483.

15 Nakamae, S., Kimura, D., Miyakoda, M., Sukhbaatar, O., Inoue, S. I., and Yui, K. 2019. Role of IL-10 in inhibiting protective immune responses against infection with heterologous *Plasmodium* parasites. *Parasitol Int* 70:5. 16

16 Lutz, M. B., Kukutsch, N., Ogilvie, A. L., Rossner, S., Koch, F., Romani, N., and Schuler, G. 1999. An advanced culture method for generating large quantities of highly pure dendritic cells from mouse bone marrow. *J Immunol Methods* 223:77.

17 Bayarsaikhan, G., Miyakoda, M., Yamamoto, K., Kimura, D., Akbari, M., Yuda, M., and Yui, K. 2017. Activation and exhaustion of antigen-specific $CD8^+$ T cells occur in different splenic compartments during infection with *Plasmodium berghei*. *Parasitol Int* 66:227.

18 Sukhbaatar, O., Kimura, D., Miyakoda, M., Nakamae, S., Kimura, K., Hara, H., Yoshida, H., Inoue, S. I., and Yui, K. 2020. Activation and IL-10 production of specific $CD4^+$ T cells are regulated by IL-27 during chronic infection with *Plasmodium chabaudi*. *Parasitol Int* 74:101994.

19 Miyakoda, M., Kimura, D., Honma, K., Kimura, K., Yuda, M., and Yui, K. 2012. Development of memory $CD8^+$ T cells and their recall responses during blood-stage infection with *Plasmodium berghei* ANKA. *J Immunol* 189:4396. 20

20 Kolde, R. 2019. pheatmap: Pretty Heatmaps. In.

21 Subramanian, A., Tamayo, P., Mootha, V. K., Mukherjee, S., Ebert, B. L., Gillette, M. A., Paulovich, A., Pomeroy, S. L., Golub, T. R., Lander, E. S., and Mesirov, J. P. 2005. Gene set enrichment analysis: a knowledge-based approach for interpreting genome-wide expression profiles. *Proc Natl Acad Sci U S A* 102:15545.

22 Marshall, H. D., Chandele, A., Jung, Y. W., Meng, H., Poholek, A. C., Parish, I. A., Rutishauser, R., Cui, W., Kleinstein, S. H., Craft, J., and Kaech, S. M. 2011. Differential expression of Ly6C and T-bet distinguish effector and memory Th1 $CD4^+$ cell properties during viral infection. *Immunity* 35:633.

23 DeLong, J. H., Hall, A. O., Konradt, C., Coppock, G. M., Park, J., Harms Pritchard, G., and Hunter, C. A. 2018. Cytokine- and TCR-mediated regulation of T cell expression of Ly6C and Sca-1. *J Immunol* 200:1761.

24 Ryg-Cornejo, V., Ioannidis, L. J., Ly, A., Chiu, C. Y., Tellier, J., Hill, D. L., Preston, S. P., Pellegrini, M., Yu, D., Nutt, S. L., Kallies, A., and Hansen, D. S. 2016. Severe Malaria Infections Impair Germinal Center Responses by Inhibiting T Follicular Helper Cell Differentiation. *Cell Rep* 14:68.

25 Obeng-Adjei, N., Portugal, S., Tran, T. M., Yazew, T. B., Skinner, J., Li, S., Jain, A., Felgner, P. L., Doumbo, O. K., Kayentao, K., Ongoiba, A., Traore, B., and Crompton, P. D. 2015. Circulating Th1-Cell-type Tfh Cells that Exhibit Impaired B Cell Help Are Preferentially Activated during Acute Malaria in Children. *Cell Rep* 13:425.

26 Haque, A., Best, S. E., Ammerdorffer, A., Desbarrieres, L., de Oca, M. M., Amante, F. H., de Labastida Rivera, F., Hertzog, P., Boyle, G. M., Hill, G. R., and Engwerda, C. R. 2011. Type I interferons suppress $CD4^+$ T-cell-dependent parasite control during blood-stage *Plasmodium* infection. *Eur J Immunol* 41:2688.

27 Ball, E. A., Sambo, M. R., Martins, M., Trovoada, M. J., Benchimol, C., Costa, J., Antunes Goncalves, L., Coutinho, A., and Penha-Goncalves, C. 2013. IFNAR1 controls progression to cerebral malaria in children and $CD8^+$ T cell brain pathology in *Plasmodium berghei*-infected mice. *J Immunol* 190:5118.

28 Aucan, C., Walley, A. J., Hennig, B. J., Fitness, J., Frodsham, A., Zhang, L., Kwiatkowski, D., and Hill, A. V. 2003. Interferon-α receptor-1 (IFNAR1) variants are associated with protection against cerebral malaria in the Gambia. *Genes Immun* 4:275.

29 Rocha, B. C., Marques, P. E., Leoratti, F. M. S., Junqueira, C., Pereira, D. B., Antonelli, L., Menezes, G. B., Golenbock, D. T., and Gazzinelli, R. T. 2015. Type I Interferon Transcriptional Signature in Neutrophils and Low-Density Granulocytes Are Associated with Tissue Damage in Malaria. *Cell Rep* 13:2829.

30 Zander, R. A., Guthmiller, J. J., Graham, A. C., Pope, R. L., Burke, B. E., Carr, D. J., and Butler, N. S. 2016. Type I interferons induce T regulatory 1 responses and restrict humoral immunity during experimental malaria. *PLoS Pathog* 12:e1005945.

31 Sebina, I., James, K. R., Soon, M. S., Fogg, L. G., Best, S. E., Labastida Rivera, F., Montes de Oca, M., Amante, F. H., Thomas, B. S., Beattie, L., Souza-Fonseca-

Guimaraes, F., Smyth, M. J., Hertzog, P. J., Hill, G. R., Hutloff, A., Engwerda, C. R., and Haque, A. 2016. IFNAR1-signalling obstructs ICOS-mediated humoral immunity during non-lethal blood-stage *Plasmodium* infection. *PLoS Pathog* 12:e1005999.

32 deWalick, S., Amante, F. H., McSweeney, K. A., Randall, L. M., Stanley, A. C., Haque, A., Kuns, R. D., MacDonald, K. P., Hill, G. R., and Engwerda, C. R. 2007. Cutting edge: conventional dendritic cells are the critical APC required for the induction of experimental cerebral malaria. *J Immunol* 178:6033.

33 Yu, X., Cai, B., Wang, M., Tan, P., Ding, X., Wu, J., Li, J., Li, Q., Liu, P., Xing, C., Wang, H. Y., Su, X. Z., and Wang, R. F. 2016. Cross-regulation of two type I interferon signaling pathways in plasmacytoid dendritic cells controls anti-malaria immunity and host mortality. *Immunity* 45:1093.

34 Spaulding, E., Fooksman, D., Moore, J. M., Saidi, A., Feintuch, C. M., Reizis, B., Chorro, L., Daily, J., and Lauvau, G. 2016. STING-Licensed Macrophages Prime Type I IFN Production by Plasmacytoid Dendritic Cells in the Bone Marrow during Severe Plasmodium yoelii Malaria. *PLoS Pathog* 12:e1005975.

35 Gallego-Marin, C., Schrum, J. E., Andrade, W. A., Shaffer, S. A., Giraldo, L. F., Lasso, A. M., Kurt-Jones, E. A., Fitzgerald, K. A., and Golenbock, D. T. 2018. Cyclic GMP-AMP Synthase Is the Cytosolic Sensor of *Plasmodium falciparum* Genomic DNA and Activates Type I IFN in Malaria. *J Immunol* 200:768.

36 Hu, Z., Blackman, M. A., Kaye, K. M., and Usherwood, E. J. 2015. Functional heterogeneity in the $CD4^+$ T cell response to murine γ-herpesvirus 68. *J Immunol* 194:2746.

37 Dumont, F. J., Palfree, R. G., and Coker, L. Z. 1986. Phenotypic changes induced by interferon in resting T cells: major enhancement of Ly-6 antigen expression. *J Immunol* 137:201.

38 Huber, J. P. and Farrar, J. D. 2011. Regulation of effector and memory T-cell functions by type I interferon. *Immunology* 132:466.

Figure legends

Figure 1.

Pcc-infection promotes Th1-biased PbT-II cell activation compared with PbA infection.

B6 mice were adoptively injected with PbT-II cells and uninfected (Uninf) or infected with PbA or Pcc on the following day. Spleen cells were isolated 7 days after infection, stained with antibodies, and analyzed using flow cytometry. (A) Representative plots (left) and summary graphs (right) of the surface staining are shown for CD4/CD45.1 on $CD4^+$ cells and for CD11a/CD49d, Ly6C/CD49d, PD-1/CXCR5 on PbT-II ($CD4^+CD45.1^+$) cells. The total number of PbT-II cells was calculated by multiplying the number of spleen cells by the ratio of $CD4^+$ T cells and the ratio of PbT-II cells in $CD4^+$ T cells. (B) Representative plots (left) and summary graphs (right) of the intracellular staining are shown for Tcf-1/T-bet and Bcl6/T-bet in PbT-II cells and LyC6 histograms of $T\text{-}bet^{hi}Tcf1^{lo}$ and $Tbet^{lo}Tcf1^{hi}$ PbT-II cells. The numbers in each graph are the proportions (%) of the indicated subpopulations. (C) The proportions of subpopulations of PbT-II cells (upper panel) and $Ly6C^+$ cells in the PbT-II subsets (lower panel) are plotted in relation to parasitemia levels on day 7. Each dot represents an individual mouse infected with PbA (red) or Pcc (blue). Pearson's correlation (two-tailed) coefficients (r) and p values are shown. Data were pooled from three independent experiments with three mice from each infection group. Two-tailed Student's *t*-test was used to compare PbA- vs. Pcc-infected mice. *p <0.05; **p <0.01; ***p <0.001; ****p <0.0001; ns p >0.05. Data are shown as mean ± SD.

Figure 2.

The proportion of IFNγ-producing PbT-II cells in Pcc-infected mice was higher than that in PbA-infected mice. B6 mice were adoptively transferred with PbT-II cells (day -1) and infected with PbA or Pcc. Mice were sacrificed, and spleen cells were harvested on day 7 after infection for intracellular cytokine staining. Spleen cells were cultured with PbT-II peptide or PMA/ionomycin; stained for CD3, CD4, and CD45.1; permeabilized; stained for intracellular IFN-γ/TNF-α (A) and IFN-γ/IL-2 (B); and analyzed using flow cytometry. Representative plots and summary graphs of the proportions of IFN-γ^+, TNF-α^+, and IFN-γ^+TNF-α^+ PbT-II cells (A) and of IL-2^+ and IFN-γ^+IL-2^+ PbT-II cells (B) are shown. Two-way ANOVA with Bonferroni's test was used to compare PbA- vs. Pcc-infected mice. *p <0.05; **p <0.01; ns p >0.05. Data are shown as the mean ± SD.

Figure 3.

Type I IFN-regulated genes are expressed at higher levels in PbT-II cells from PbA-infected mice than those from Pcc-infected mice. B6 mice were adoptively transferred with PbT-II cells and infected with PbA the following day (n = 3). Seven days after infection, CD11a^{hi}CD49d^{hi} and CD11a^{hi}CD49d^{lo} PbT-II cells were sorted from individual mice; RNA was subjected to microarray analysis (A-F). Results were analyzed with those from CD11a^{lo}CD49d^{lo} cells from uninfected mice (n = 4) and those from CD11a^{hi}CD49d^{hi} and CD11a^{hi}CD49d^{lo} PbT-II cells from Pcc-infected mice (n = 3) (12). (A) Principal component analysis (PCA) of CD11a^{lo}CD49d^{lo} PbT-II cells from uninfected mice (black), CD11a^{hi}CD49d^{hi} (red) and CD11a^{hi}CD49d^{lo} (purple) cells from PbA-infected mice, and CD11a^{hi}CD49d^{hi} (green) and CD11a^{hi}CD49d^{lo} (blue) cells from Pcc-infected mice. The plots are shown at two different angles. Each dot represents the PbT-II cells prepared from one mouse. (B) Venn diagram showing the total number of DEGs and shared genes within CD11a^{hi}CD49d^{hi} (yellow) and CD11a^{hi}CD49d^{lo} (red) PbT-II cells between PbA- and Pcc-infected mice. (C) Heatmap of the top 10 DEGs in CD11a^{hi}CD49d^{hi} PbT-II cells (upper panel) and representative Th1- and Tfh-related genes (middle panel and lower panel, respectively). Type I IFN-related genes are highlighted in red. (D) Volcano plots of DEGs in CD11a^{hi}CD49d^{hi} (left) and CD11a^{hi}CD49d^{lo} (right) PbT-II cells from PbA- and Pcc-infected mice (red and blue, respectively; FDR < 0.05). (E) Gene ontology (GO) of DEGs in CD11a^{hi}CD49d^{hi} (upper panel) and CD11a^{hi}CD49d^{lo} (lower panel) cells. (F) Enrichment plots obtained from GSEA of DEGs in CD11a^{hi}CD49d^{hi} (left panel) and CD11a^{hi}CD49d^{lo} (right panel) PbT-II cells. (G) B6 mice were infected with PbA (n = 10) or Pcc (n = 9), and their spleens were weighed and lysed 5 days later. The concentrations of IFN-α and IFN-γ in spleen lysates were determined using ELISA. Two-tailed Student's *t*-test was used to compare PbA- vs. Pcc-infected mice. ****p <0.0001; ns p >0.05. Data are shown as mean ± SD.

Figure 4.

Inhibition of type I IFN signaling modulates CD4^{+} T-cell responses during infection with PbA. B6 mice were adoptively transferred with PbT-II cells, infected with PbA on the next day, and treated with anti-IFNAR1 blocking mAb (black) or IgG (red) on days 0, 2, and 4 after infection. Parasitemia was monitored (A). Spleen cells were prepared 7 days after infection, stained with mAbs, and analyzed using flow cytometry. (B, C)

Representative plots and summary graphs for CD45.2/CD45.1 in $CD4^+$ cells (B) and for CD11a/CD49d and Ly6C/CD49d in PbT-II and host $CD4^+$ T cells (C). The total number of PbT-II cells was calculated by multiplying the number of spleen cells with the ratio of PbT-II cells in each spleen. (D) Representative plots and summary graphs of the intracellular staining for T-bet /Tcf1, and LyC6 in $T\text{-}bet^{hi}Tcf1^{lo}$ and $Tbet^{lo}Tcf1^{hi}$ PbT-II and host $CD4^+$ T cells. Representative results of 2 experiments with similar results are shown. A two-tailed Student's *t*-test was used for comparison (B-D). Two-way ANOVA followed by Bonferroni test was used to compare IgG- and anti-IFNAR1 mAb-treated mice (E). **p* <0.05; ***p* <0.01; ****p* <0.001; *****p* <0.0001; ns *p* >0.05.

Figure 5.

The levels of memory PbT-II T cells induced by infection with PbA are higher than those induced with Pcc infection. (A-C) B6 mice were transferred with PbT-II cells, infected with PbA (red) or Pcc (blue) on the following day, treated with chloroquine and sulfadiazine between days 6 and 15. Spleen cells were prepared on day 21, stained with mAbs, and analyzed using flow cytometry. Representative plots (upper) and summary graphs (lower) of the staining for CD45.2/CD45.1 in $CD4^+$ cells and for CD11a/CD49d, Ly6C/CD49d, PD-1/CXCR5, CD127/KLRG1 (A) and CD62L/CD44 (B) in PbT-II ($CD4^+CD45.1^+$) cells. The total number of PbT-II cells was calculated by multiplying the number of spleen cells with the ratio of PbT-II cells. Representative plots (upper) and summary graphs (lower) of the intracellular staining are shown for Tcf-1/T-bet and Bcl6/CXCR5 in PbT-II cells (C). Two-tailed Student's *t*-test was used for the statistical analysis. **p* <0.05; ***p* <0.01; ns *p* >0.05 (D) B6 mice were infected with PbA (red) or Pcc (blue) and treated with chloroquine and sulfadiazine between days 6 and 15, and serum samples were collected on day 22. The levels of PbA- and Pcc-specific IgM, IgG1, IgG2b, and IgG2c were determined using ELISA. Representative results of 2 experiments with similar results are shown. Multiple Student's *t*-test was used for the statistical analysis. **p* <0.05; ***p* <0.01; ns *p* >0.05

Figure 6.

The recall response of memory PbT-II T cells in PbA- and Pcc-primed mice are not significantly different after infection with PbA. B6 mice were transferred with PbT-II cells, infected with PbA (red) or Pcc (blue), and treated with chloroquine and sulfadiazine

as in Fig. 5. (A-C) Mice were immunized with BM-DCs pulsed with PbT-II peptide on day 22 of the infection. Experimental design (A). The proportions of PbT-II cells in $CD4^+$ T cells ($CD45.1^+$ cells/$CD4^+$ cells) were monitored in peripheral blood (B). Fourteen days after immunization, the proportions of PbT-II cells in $CD4^+$ T cells and the total numbers in the spleen were determined (C). (D-F) The PbA- and Pcc-infected and anti-malarial treated mice were re-infected with PbA 21 days after the first infection, and parasitemia levels were monitored (D). Seven days after PbA infection, spleen cells were stained with antibodies and analyzed using flow cytometry. Representative plots (upper) and summary graphs (lower) of the surface staining for CD45.2/CD45.1 in $CD4^+$ cells and CD11a/CD49d and PD-1/CXCR5 in PbT-II ($CD4^+CD45.1^+$) cells (E). Representative plots (upper) and summary graphs (lower) of the intracellular staining for Tcf-1/T-bet and Bcl6/CXCR5 in PbT-II cells (F). The total number of PbT-II cells was calculated as in Fig. 5. Representative results of 2 experiments with similar results are shown. Two-tailed Student's *t*-test was used for the statistical analysis. ns $p > 0.05$. The data are shown as the mean ± SD.

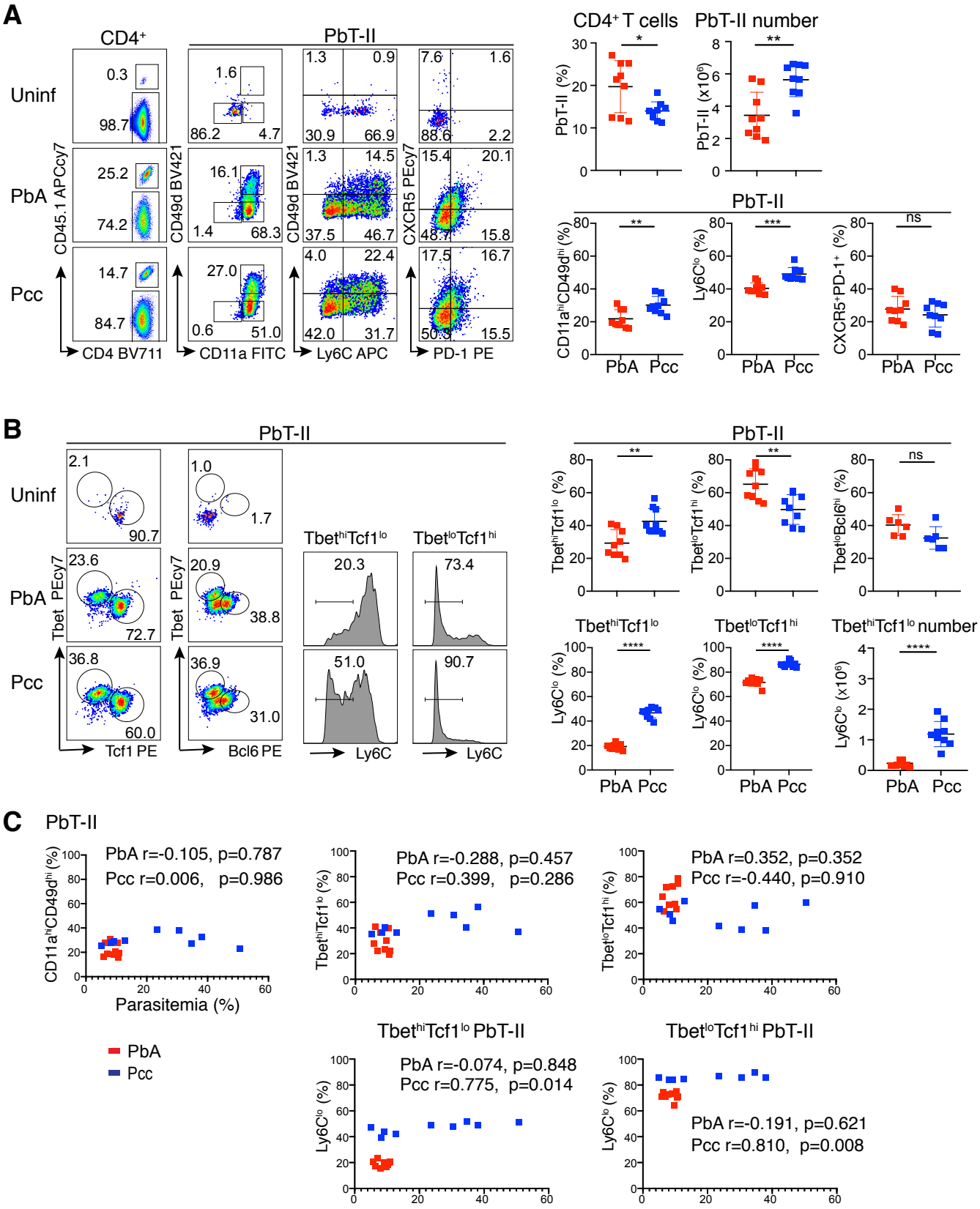
A
CD4+
PbT-II
Uninf
PbA
Pcc
CD45.1 APCcy7
CD49d BV421
CXCR5 PEcy7
CD4 BV711
CD11a FITC
Ly6C APC
PD-1 PE
CD4+ T cells
PbT-II number
PbT-II (%)
PbT-II (x10^6)
CD11a^hiCD49d^hi (%)
Ly6C^lo (%)
CXCR5+PD-1+ (%)
PbA
Pcc
ns
B
Tbet PEcy7
Tcf1 PE
Bcl6 PE
Tbet^hiTcf1^lo
Tbet^loTcf1^hi
Ly6C
Tbet^hiTcf1^lo (%)
Tbet^loTcf1^hi (%)
Tbet^loBcl6^hi (%)
Ly6C^lo (%)
Tbet^hiTcf1^lo number
Ly6C^lo (x10^6)
C
PbT-II
CD11a^hiCD49d^hi (%)
PbA r=-0.105, p=0.787
Pcc r=0.006, p=0.986
Parasitemia (%)
PbA
Pcc
Tbet^hiTcf1^lo (%)
PbA r=-0.288, p=0.457
Pcc r=0.399, p=0.286
Tbet^loTcf1^hi (%)
PbA r=0.352, p=0.352
Pcc r=-0.440, p=0.910
Tbet^hiTcf1^lo PbT-II
Ly6C^lo (%)
PbA r=-0.074, p=0.848
Pcc r=0.775, p=0.014
Tbet^loTcf1^hi PbT-II
PbA r=-0.191, p=0.621
Pcc r=0.810, p=0.008

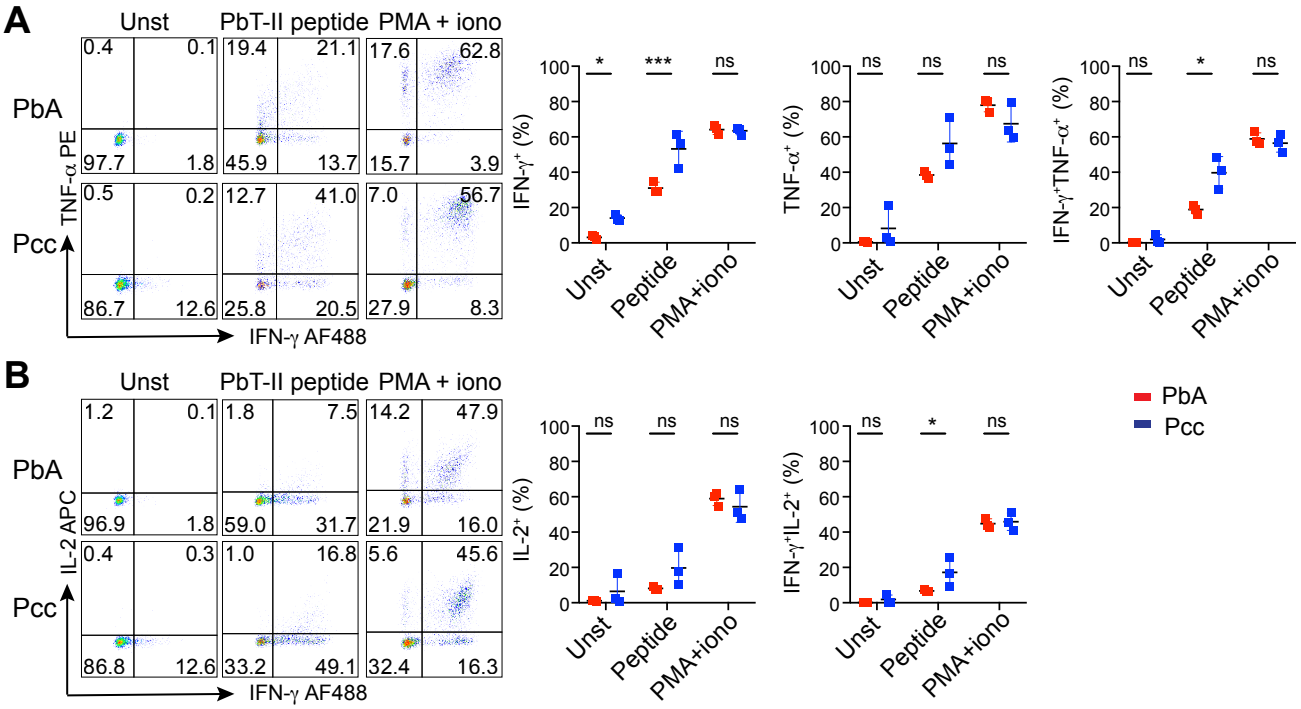
A
Unst
PbT-II peptide
PMA + iono
PbA
Pcc
TNF-α PE
IFN-γ AF488
0.4
0.1
97.7
1.8
19.4
21.1
45.9
13.7
17.6
62.8
15.7
3.9
0.5
0.2
86.7
12.6
12.7
41.0
25.8
20.5
7.0
56.7
27.9
8.3
IFN-γ+ (%)
TNF-α+ (%)
IFN-γ+TNF-α+ (%)
*
***
ns
Unst
Peptide
PMA+iono

B
Unst
PbT-II peptide
PMA + iono
PbA
Pcc
IL-2 APC
IFN-γ AF488
1.2
0.1
96.9
1.8
1.8
7.5
59.0
31.7
14.2
47.9
21.9
16.0
0.4
0.3
86.8
12.6
1.0
16.8
33.2
49.1
5.6
45.6
32.4
16.3
IL-2+ (%)
IFN-γ+IL-2+ (%)
ns
*
Unst
Peptide
PMA+iono
PbA
Pcc

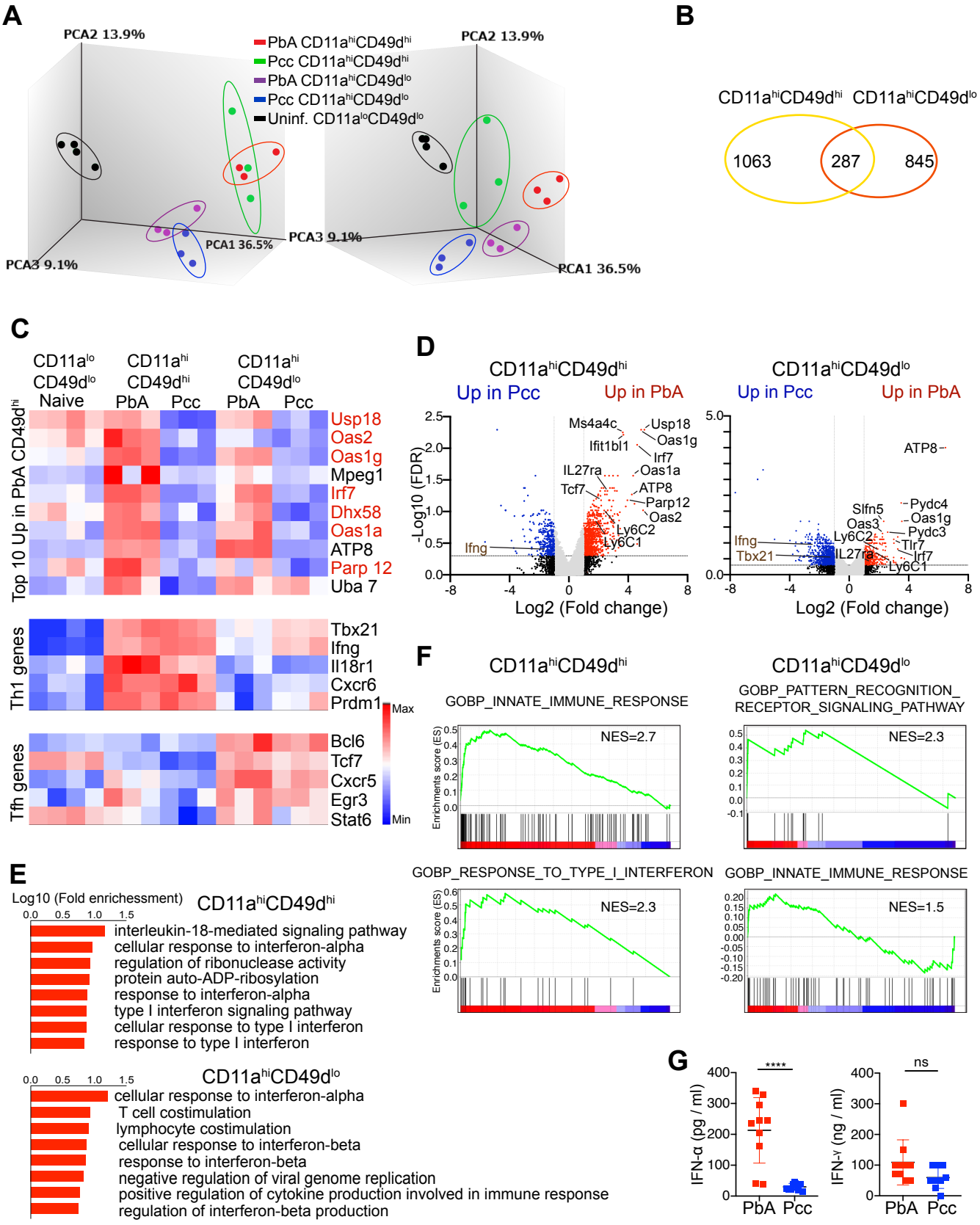
A
PCA2 13.9%
PbA CD11a^hiCD49d^hi
Pcc CD11a^hiCD49d^hi
PbA CD11a^hiCD49d^lo
Pcc CD11a^hiCD49d^lo
Uninf. CD11a^loCD49d^lo
PCA1 36.5%
PCA3 9.1%
B
CD11a^hiCD49d^hi
CD11a^hiCD49d^lo
1063
287
845
C
CD11a^lo CD49d^lo Naive
CD11a^hi CD49d^hi PbA
CD11a^hi CD49d^lo PbA
CD11a^hi CD49d^lo Pcc
Top 10 Up in PbA CD49d^hi
Usp18
Oas2
Oas1g
Mpeg1
Irf7
Dhx58
Oas1a
ATP8
Parp 12
Uba 7
Th1 genes
Tbx21
Ifng
Il18r1
Cxcr6
Prdm1
Tfh genes
Bcl6
Tcf7
Cxcr5
Egr3
Stat6
Max
Min
D
CD11a^hiCD49d^hi
Up in Pcc
Up in PbA
-Log10 (FDR)
Log2 (Fold change)
Ms4a4c
Usp18
Ifit1bl1
Oas1g
Irf7
IL27ra
Oas1a
Tcf7
ATP8
Parp12
Oas2
Ly6C2
Ly6C1
Ifng
CD11a^hiCD49d^lo
Up in Pcc
Up in PbA
ATP8
Slfn5
Pydc4
Oas3
Oas1g
Ly6C2
Pydc3
Ifng
Tlr7
Tbx21
IL27ra
Irf7
Ly6C1
Log2 (Fold change)
E
Log10 (Fold enrichessment)
CD11a^hiCD49d^hi
interleukin-18-mediated signaling pathway
cellular response to interferon-alpha
regulation of ribonuclease activity
protein auto-ADP-ribosylation
response to interferon-alpha
type I interferon signaling pathway
cellular response to type I interferon
response to type I interferon
CD11a^hiCD49d^lo
cellular response to interferon-alpha
T cell costimulation
lymphocyte costimulation
cellular response to interferon-beta
response to interferon-beta
negative regulation of viral genome replication
positive regulation of cytokine production involved in immune response
regulation of interferon-beta production
F
CD11a^hiCD49d^hi
GOBP_INNATE_IMMUNE_RESPONSE
NES=2.7
CD11a^hiCD49d^lo
GOBP_PATTERN_RECOGNITION_ RECEPTOR_SIGNALING_PATHWAY
NES=2.3
GOBP_RESPONSE_TO_TYPE_I_INTERFERON
NES=2.3
GOBP_INNATE_IMMUNE_RESPONSE
NES=1.5
Enrichments score (ES)
G
IFN-α (pg / ml)
****
PbA
Pcc
IFN-γ (ng / ml)
ns
PbA
Pcc

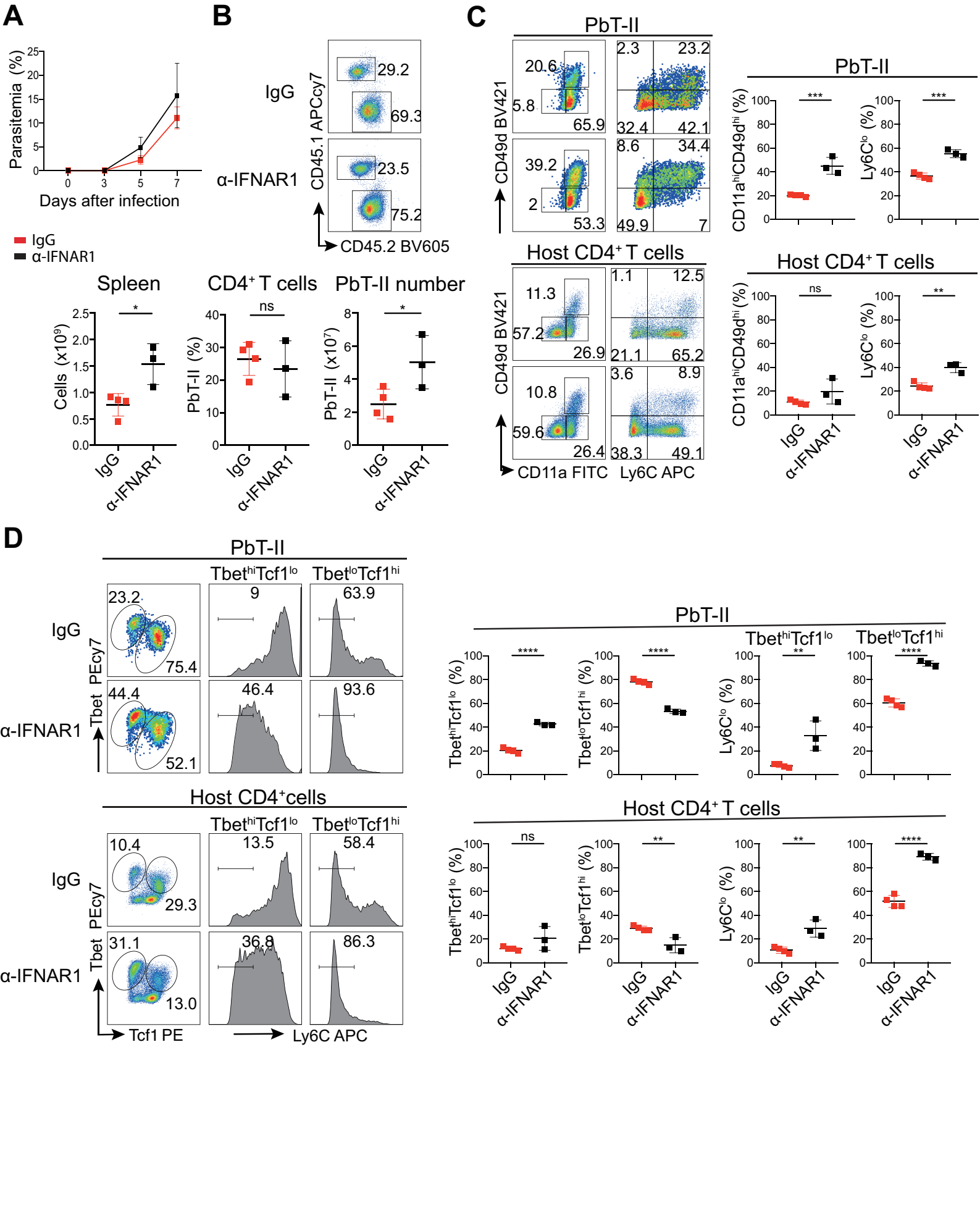
A
Parasitemia (%)
Days after infection
IgG
α-IFNAR1
B
IgG
α-IFNAR1
CD45.1 APCcy7
CD45.2 BV605
29.2
69.3
23.5
75.2
Spleen
CD4+ T cells
PbT-II number
Cells (x10^9)
PbT-II (%)
PbT-II (x10^7)
ns
C
PbT-II
Host CD4+ T cells
CD49d BV421
CD11a FITC
Ly6C APC
20.6
5.8
65.9
2.3
23.2
32.4
42.1
39.2
2
53.3
8.6
34.4
49.9
7
11.3
57.2
26.9
1.1
12.5
21.1
65.2
10.8
59.6
26.4
3.6
8.9
38.3
49.1
CD11a^hiCD49d^hi (%)
Ly6C^lo (%)
D
PbT-II
Host CD4+cells
Host CD4+ T cells
Tbet PEcy7
Tcf1 PE
Ly6C APC
Tbet^hiTcf1^lo
Tbet^loTcf1^hi
23.2
75.4
44.4
52.1
9
63.9
46.4
93.6
10.4
29.3
31.1
13.0
13.5
58.4
36.8
86.3
Tbet^hiTcf1^lo (%)
Tbet^loTcf1^hi (%)
Ly6C^lo (%)

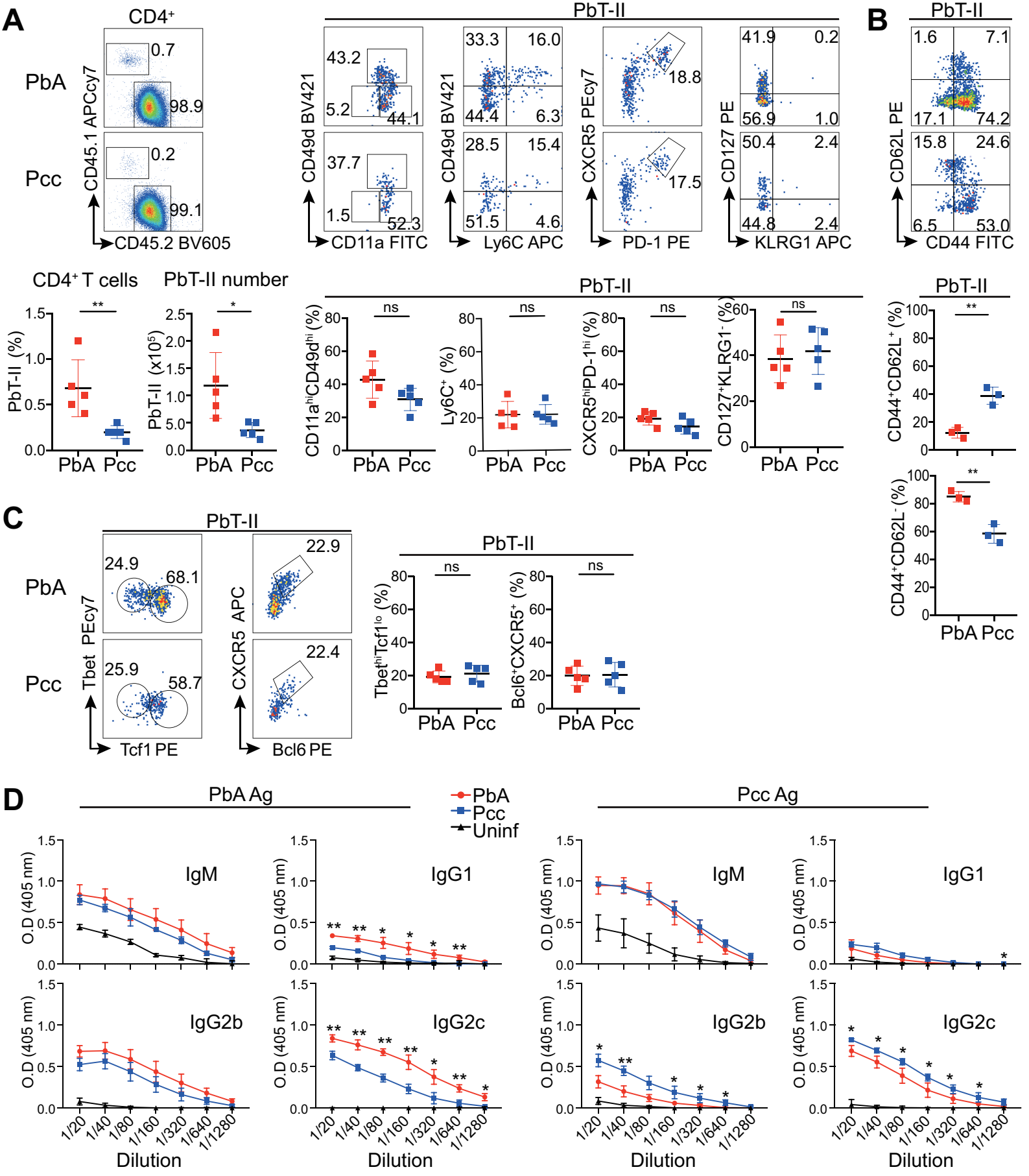
A
CD4+
PbA
Pcc
0.7
98.9
0.2
99.1
CD45.1 APCcy7
CD45.2 BV605
PbT-II
43.2
5.2
44.1
37.7
1.5
52.3
CD49d BV421
CD11a FITC
33.3
16.0
44.4
6.3
28.5
15.4
51.5
4.6
Ly6C APC
18.8
17.5
CXCR5 PEcy7
PD-1 PE
41.9
0.2
56.9
1.0
50.4
2.4
44.8
2.4
CD127 PE
KLRG1 APC
B
PbT-II
1.6
7.1
17.1
74.2
15.8
24.6
6.5
53.0
CD62L PE
CD44 FITC
CD4+ T cells
PbT-II number
PbT-II (%)
PbT-II (x10^5)
**
*
PbA Pcc
PbT-II
ns
CD11a^hiCD49d^hi (%)
Ly6C+ (%)
CXCR5^hiPD-1^hi (%)
CD127+KLRG1- (%)
CD44+CD62L+ (%)
CD44+CD62L- (%)
C
PbT-II
PbA
Pcc
24.9
68.1
25.9
58.7
Tbet PEcy7
Tcf1 PE
22.9
22.4
CXCR5 APC
Bcl6 PE
Tbet^hiTcf1^lo (%)
Bcl6+CXCR5+ (%)
D
PbA Ag
Pcc Ag
PbA
Pcc
Uninf
IgM
IgG1
IgG2b
IgG2c
O.D (405 nm)
1/20
1/40
1/80
1/160
1/320
1/640
1/1280
Dilution

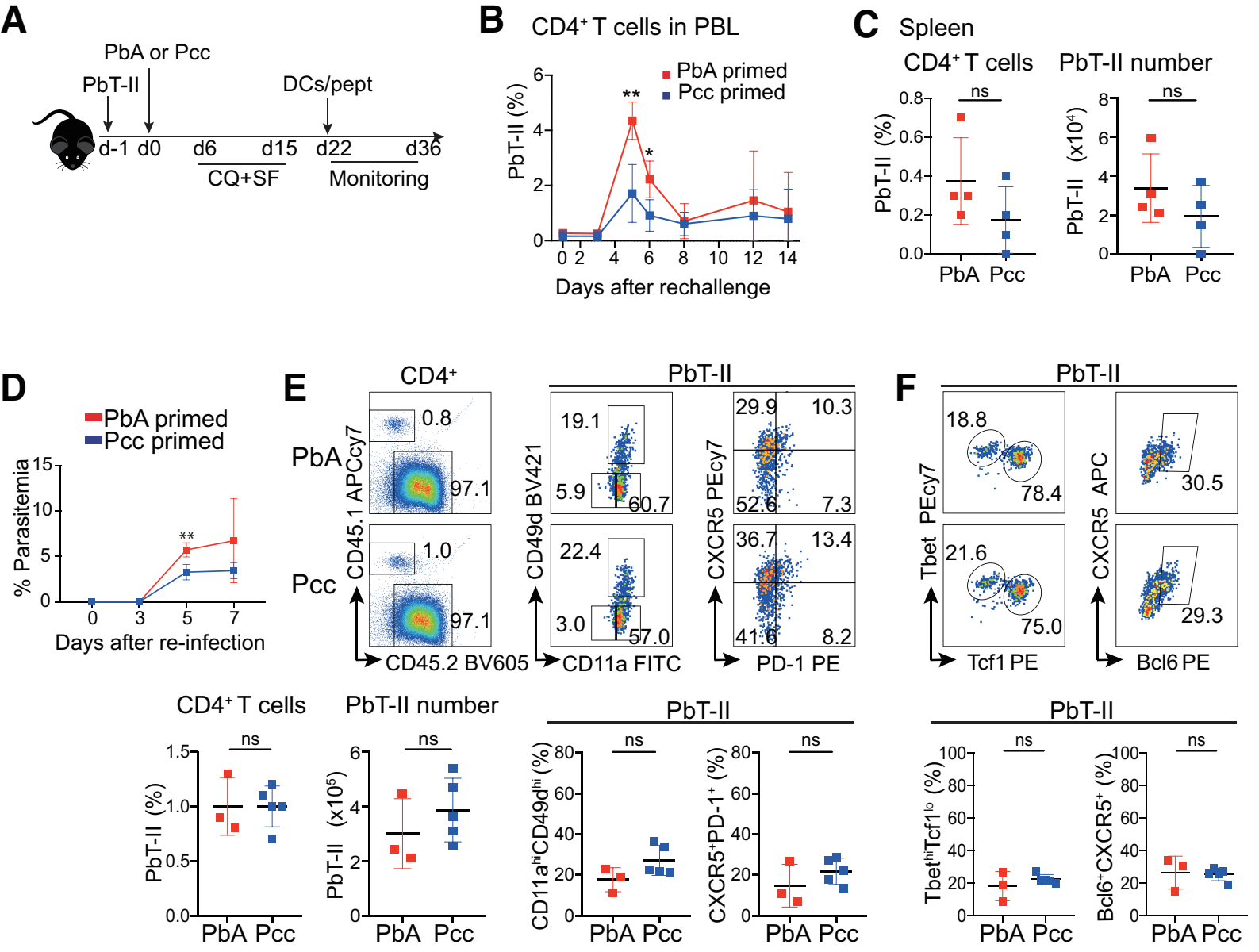
A
PbA or Pcc
PbT-II
DCs/pept
d-1 d0 d6 d15 d22 d36
CQ+SF
Monitoring
B
CD4+ T cells in PBL
PbA primed
Pcc primed
PbT-II (%)
Days after rechallenge
C
Spleen
CD4+ T cells
PbT-II number
PbT-II (%)
PbT-II (x10⁴)
ns
PbA Pcc
D
PbA primed
Pcc primed
% Parasitemia
Days after re-infection
E
CD4+
PbT-II
PbA
Pcc
CD45.1 APCcy7
CD45.2 BV605
CD49d BV421
CD11a FITC
CXCR5 PEcy7
PD-1 PE
F
PbT-II
Tbet PEcy7
Tcf1 PE
CXCR5 APC
Bcl6 PE
CD4+ T cells
PbT-II number
PbT-II (%)
PbT-II (x10⁵)
CD11a^hiCD49d^hi (%)
CXCR5+PD-1+ (%)
Tbet^hiTcf1^lo (%)
Bcl6+CXCR5+ (%)